Kondo behavior, ferromagnetic correlations, and crystal fields in the heavy-fermion compounds Ce_3X (X=In,Sn)

C. H. Wang,[1,2] J. M. Lawrence,[1] A. D. Christianson,[3] E. A. Goremychkin,[4] V. R. Fanelli,[2] K. Gofryk,[2] E. D. Bauer,[2] F. Ronning,[2] J. D. Thompson,[2] N. R. de Souza,[4,5] A. I. Kolesnikov,[3] and K. C. Littrell[3]

[1]*University of California, Irvine, California 92697, USA*

[2]*Los Alamos National Laboratory, Los Alamos, New Mexico 87545, USA*

[3]*Neutron Scattering Sciences Division, Oak Ridge National Laboratory, Oak Ridge, Tennessee 37831, USA*

[4]*Argonne National Laboratory, Argonne, Illinois 60439, USA*

[5]*Australian Nuclear Science and Technology Organisation, Lucas Heights, New South Wales 2234, Australia*

(Received 9 March 2010; revised manuscript received 19 May 2010; published 25 June 2010)

We report measurements of inelastic neutron scattering, magnetic susceptibility, magnetization, and the magnetic field dependence of the specific heat for the heavy Fermion compounds Ce_3In and Ce_3Sn. The neutron scattering results show that the excited crystal field levels have energies E_1=13.2 meV, E_2=44.8 meV for Ce_3In and E_1=18.5 meV, E_2=36.1 meV for Ce_3Sn. The Kondo temperature deduced from the quasielastic linewidth is 17 K for Ce_3In and 40 K for Ce_3Sn. The low-temperature behavior of the specific heat, magnetization, and susceptibility cannot be well described by J=1/2 Kondo physics alone, but require calculations that include contributions from the Kondo effect, broadened crystal fields, and ferromagnetic correlations, all of which are known to be important in these compounds. We find that in Ce_3In the ferromagnetic fluctuation makes a 10%–15% contribution to the ground state doublet entropy and magnetization. The large specific heat coefficient γ in this heavy fermion system thus arises more from the ferromagnetic correlations than from the Kondo behavior.

DOI: 10.1103/PhysRevB.81.235132 PACS number(s): 71.27.+a, 71.70.Ch, 75.20.Hr

I. INTRODUCTION

In heavy fermion (HF) compounds, it is very common to establish the Kondo energy scale T_K from the linear coefficient of specific heat γ through Rajan's formula $T_K=\pi JR/3\gamma_0$ derived for the degenerate $(2J+1\geq 2)$ Kondo model[1] where J is the total angular momentum. In previous studies of the specific heat of the HF compounds Ce_3X (X=In,Sn) (Refs. 2 and 3), which crystallize in the Cu_3Au cubic structure, this formula was used to determine the Kondo temperature, which was found to be 4.8 K for Ce_3In and 16.7 K for Ce_3Sn. The crystal electric field (CEF) excitation energy was estimated to be T_{CEF}=65 K.

Most HF compounds reside close to a quantum critical point (QCP) where antiferromagnetic (AFM) or ferromagnetic (FM) correlations are present. This makes the previous analysis inappropriate in so far as it assumes that the magnetic correlations do not contribute to γ. Indeed, the Wilson ratios $(\pi^2R\chi_0/3C_J\gamma_0)$ which were determined previously for Ce_3In and Ce_3Sn are 11.5 and 7.0, respectively,[2,3] indicating that ferromagnetic correlations dominate the susceptibility.

Inelastic neutron scattering (INS) experiments on single crystals of compounds that are close to a QCP, such as $CeRu_2Si_2$ (Ref. 4) or $CeNi_2Ge_2$,[5] exhibit two classes of excitations. In the reciprocal-lattice space, at most wave vectors **Q** in the Brillouin zone, the scattering has the characteristic Kondo energy dependence and is **Q** independent or only weakly **Q** dependent. Similar behavior is observed in intermediate valence compounds for which it is clear that the behavior of the low temperature susceptibility, specific heat and INS spectra are close to the Kondo impurity prediction, as though the onset of lattice coherence has only a minor effect on these measurements.[6,7] Near the QCP, however, large **Q**-dependent scattering is observed with maximum intensity at the critical wave vector $\mathbf{Q}_c$ ($\mathbf{Q}_c$=0 for FM and $\mathbf{Q}_c=\mathbf{Q}_N$ for AFM) where ordering occurs in the nearby magnetic state. This scattering represents the short range order. It is dynamic and critically slows down, or softens, as the QCP is approached by lowering the temperature or changing a control parameter. These fluctuations affect the specific heat and can result in non-Fermi liquid behavior.

Hence, INS in single crystals can separate the Kondo behavior from the contributions due to magnetic correlations. For INS in polycrystalline samples, the momentum is averaged over a sphere of constant $Q=|\mathbf{Q}|$, and since the spectral weight in the magnetic correlations is typically small, the INS will be dominated by the Q-independent Kondo scattering. INS can also be used to directly determine the CEF excitations. Under these circumstance, INS provides a better way to determine T_K and E_{CEF} than through analysis of the specific heat. In this paper, we employ INS to determine both T_K and E_{CEF}. We have remeasured the magnetic susceptibility, and have extended the specific heat measurement, which in the previous report was measured down to 1.8 K in zero applied magnetic field, to T=400 mK and B=9 T. We have also measured the low-temperature magnetization to 13 T.

In the Ce_3X compounds, the Ce ions sit on the face centers of the cubic lattice and are subject to a crystalline electric field (CEF) of tetragonal symmetry. In this case, the Hamiltonian is described as:

$$H_{CF}=B_2^0O_2^0+B_4^0O_4^0+B_4^4O_4^4,$$

where B_l^m and O_l^m are the crystal field parameters and Steven operators, respectively. The sixfold degenerate $4f^1$, J=5/2 state splits into three doublets. Diagonalizing the Hamil-

tonian, the atomic wave functions are given by:[8,9]

$$\Gamma_7^{(1)} = \eta|\pm 5/2\rangle + \sqrt{1-\eta^2}|\mp 3/2\rangle$$

$$\Gamma_7^{(2)} = \sqrt{1-\eta^2}|\pm 5/2\rangle - \eta|\mp 3/2\rangle$$

$$\Gamma_6 = |\pm 1/2\rangle.$$

Depending on the admixture of the $J=5/2$ and 3/2 states, the inelastic neutron scattering spectra will exhibit one or two inelastic excitations. Low energy transfer quasielastic scattering will also be observed if the instrumental resolution is adequate. From the INS spectra, the crystal field energies and wave functions can be determined from the amplitudes and energies of the excitations. The Kondo effect, which arises from the hybridization of the $4f$ electron with the conduction electrons, broadens the peak line-widths proportional to $k_B T_K$. The quasielastic scattering peak width Γ_{QE} can be equated to the Kondo energy $k_B T_K$ of the ground state doublet.

In what follows, we will use the CEF parameters and the Kondo energies derived from the neutron scattering to calculate the Kondo contribution to the specific heat, susceptibility and magnetization. All the Kondo calculations utilized[1,10,11] employ the same Bethe-Ansatz method, making intercomparison possible.

II. EXPERIMENT

All samples were prepared by arc melting in an ultra-high-purity argon atmosphere. After melting, the samples were sealed under vacuum and annealed at 500 °C for 2 weeks and cooled slowly to room temperature. The magnetization was measured in a 14 T Quantum Design Vibrating Sample Magnetometer at the National High Magnetic Field Laboratory (NHMFL) at Los Alamos National Laboratory. The specific heat was measured in a Quantum Design PPMS system. The magnetic susceptibility measurements were performed in a commercial superconducting quantum interference device (SQUID) magnetometer.

We performed inelastic neutron scattering on a 29 g sample of Ce_3In and a 37 g sample of Ce_3Sn using the high energy transfer chopper spectrometer (HET) at ISIS (at the Rutherford Appleton Laboratory) and the low resolution medium energy chopper spectrometer (LRMECS) at IPNS (at Argonne National Laboratory). For Ce_3Sn, a quasi-elastic neutron spectrometer (QENS at IPNS) was also used to measure the low energy scattering. To increase the dynamic range of the INS spectrum, a variety of incident energies (E_i=15, 35, 60, and 100 meV for HET and 35 meV for LRMECS) and temperatures (4.5, 100, 150, 200, and 250 K for HET; 10, 100, and 150K for LRMECS) were employed. The HET data have been normalized to vanadium to establish the absolute value. All the data have been corrected for absorption (which is particularly significant for Ce_3In), total scattering cross section, and sample mass.

For the HET data, the low Q data were obtained from averaging the low angle detectors with angles ranging from 11.5 degrees to 26.5 degrees. The high Q data were obtained from the high angle detector bank at an angle 136 degrees. For the LRMECS experiment, the low Q data were obtained by averaging over the low angle detectors with average angle equal to 13 degrees; and the high Q data were obtained from high angle detectors where the average angle was 87 degrees. The QENS data were collected at 7 K. This inverse geometry spectrometer has 19 detector banks with Q from Q=0.36 Å^{-1} to Q=2.52 Å^{-1}, each with a slightly different final energy (E_f from 2.82 to 3.36 meV). For every fixed Q, we removed the Ce $4f$ form factor to obtain a spectrum representing the $Q=0$ scattering and then summed all 19 spectra together to obtain a total $S(Q=0,\Delta E)$ spectrum. In order to compare the QENS spectrum with the spectra from the direct geometry spectrometers HET and LRMECS, we multiplied the QENS spectrum $S(Q=0,\Delta E)$ by the $4f$ form factor appropriate for HET at E_i=35 meV.

To subtract the nonmagnetic (background, single phonon, and multiple phonon) contributions, we measured the nonmagnetic counterpart compounds La_3In and La_3Sn. For the specific heat, we obtained the magnetic contribution by direct subtraction, i.e., $C_{mag}=C(\mathrm{Ce})-C(\mathrm{La})$. For the INS data we used La_3In and La_3Sn to determine the scaling of the nonmagnetic scattering between low Q and high Q as $h(\Delta E)=S(La,LQ)/S(La,HQ)$ (LQ represents the low Q data at small scattering angle and HQ represents the high-Q data at large scattering angle). Using this factor we scaled the high Q data (where the nonmagnetic scattering dominates) to the low Q data (where the magnetic scattering dominates) for the Ce compounds to determine the nonmagnetic contribution.[7,12,13]

III. RESULTS AND ANALYSIS

In this section, we present the results of INS for Ce_3X, together with the magnetic susceptibility and specific heat, which extended to low temperature and high-magnetic field, as well as the low-temperature magnetization. We analyze the data in a manner that includes contributions from the Kondo effect, from crystal fields, and from magnetic fluctuations.

A. Ce_3In

Figures 1(a) and 1(b) directly compare the low Q INS spectra of Ce_3In and La_3In; the data were collected on HET with incident energy E_i=15 meV (a) and 60 meV (b) at 4.5 K. The spectra in (a), which compare the Ce_3In and La_3In scattering at low energy transfer ($\Delta E<9$ meV), exhibit obvious quasielastic scattering which as mentioned above arises from Kondo scattering. In Fig. 1(b), two excited energy levels, corresponding to crystal field excitations, are observed for Ce_3In. Figure 1(c) compares the low-Q and high-Q scattering obtained on LRMECS with E_i=35 meV, showing that the magnetic scattering (which decreases with Q) dominates the nonmagnetic scattering (which increases with Q).

The magnetic contribution S_{mag} to the scattering of Ce_3In, obtained using the method described above, is shown in Fig. 2. The solid lines represent a fit to the CEF model. Since the

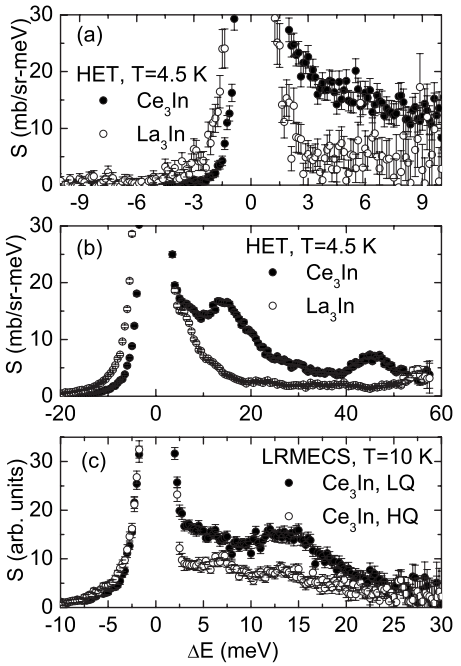

FIG. 1. Inelastic neutron scattering spectra for Ce_3In together with that of the nonmagnetic counterpart compound La_3In. The data were collected on HET and LRMECS. (a) E_i=15 meV and (b) E_i=60 meV spectra of Ce_3In and La_3In. (c) E_i=35 meV spectra at low Q and high Q for Ce_3In. The increased elastic intensity of La_3In relative to Ce_3In seen in neutron energy gain arises from the larger incoherent scattering length for La than for Ce.

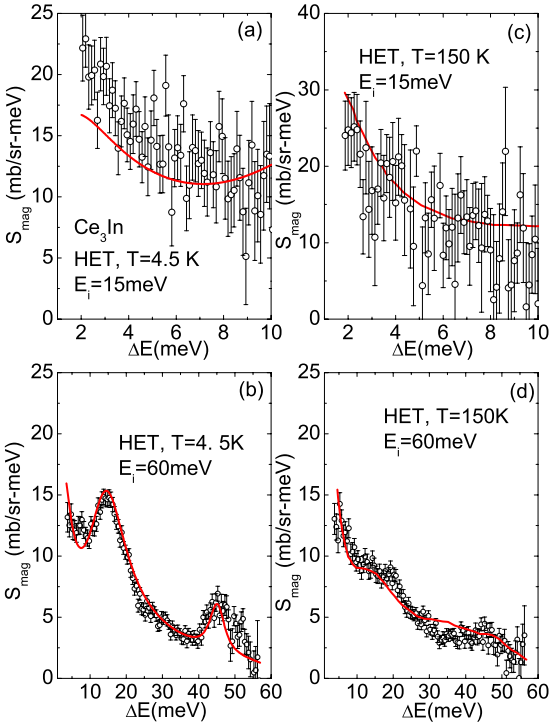

FIG. 2. (Color online) Magnetic contribution S_{mag} to the inelastic neutron scattering spectra of Ce_3In for data taken on HET at T=4.5 and 150 K with different incident energies E_i=15 and 60 meV. The solid lines represent the quasielastic and crystal field contributions obtained from least-squares fitting as described in the text.

inelastic peaks are relatively broad, the line widths Γ_i are taken to be finite. In this case, the magnetic scattering is described as:

$$S_{\mathrm{mag}} = \frac{2N}{\pi\mu_B^2} f^2(Q)(1 - e^{-\Delta E/k_B T})\chi''(Q,\Delta E)$$

$$\chi''(Q,\Delta E) = \Sigma \chi_i(T)\Delta E\left(\frac{\Gamma_i}{2\pi}\right)/[(\Delta E - E_i)^2 + \Gamma_i^2]$$

Here i=0,1,2, E_0=0 corresponds to the quasielastic scattering, and $f^2(Q)$ is the Ce $4f$ form factor. The CEF model fitting was performed simultaneously on six data sets at three different incident energies (E_i=15 meV, 35 meV and 60 meV) and at two different temperatures (4.5 and 150 K). Data for $\Delta E \leq 2$ meV (where Fig. 1(a) indicates strong elastic scattering) were excluded from the fists in Figs. 2(a) and 2(c). Figures 2(a)–2(d) exhibit fits to some of the data collected on HET. The resulting CEF fitting parameters are shown in Table I. The ground state is the $\Gamma_7^{(1)}$ doublet, the first excited state is the $\Gamma_7^{(2)}$ doublet[14] at the energy 13.2 meV, and the second excited state is the Γ_6 doublet at the energy 44.8 meV. The quasielastic line width $\Gamma_{QE}=\Gamma_0$=1.49 meV, implies that $T_K=\Gamma_{QE}/k_B$=17 K.

Due to the large CEF excitation energies, the low-temperature behavior of the magnetic specific heat should be dominated by the $\Gamma_7^{(1)}$ doublet ground state. This is confirmed by the fact that the magnetic entropy [Fig. 3(a) inset] reaches Rln2 near 20 K but only reaches Rln4 near 70 K. For a doublet ground state, the Kondo model predicts $\gamma_0=\pi R/6T_K$ for the linear coefficient of specific heat.[1] In previous results for Ce_3In a value T_K=4.8 K was deduced using this formula.[2] In addition, the specific heat coefficient C/T showed a peak near 2 K whose existence was somewhat uncertain since the lowest measured temperature was only 1.8 K. We have extended the specific heat measurement down to 400 mK. In Fig. 3(a) we plot C_{mag}/T and find a peak at T=2.6 K. Comparison of the data to the prediction $\gamma^K(T)$ of the Kondo model which is calculated using the value $T_K=\Gamma_{QE}/k_B$=17 K deduced from our neutron data, shows

TABLE I. CEF model fitting parameters for Ce_3In and Ce_3Sn.

	Ce_3In	Ce_3Sn
B_2^0(meV)	−2.203 ± 0.015	−1.660 ± 0.017
B_4^0(meV)	0.066 ± 0.001	0.038 ± 0.0009
B_4^4(meV)	−0.154 ± 0.004	−0.263 ± 0.003
η	0.94	0.89
E_1 (meV)	13.2	18.5
E_2 (meV)	44.8	36.1
Γ_{QE} (meV)	1.49 ± 0.07	3.52 ± 0.16
Γ_1 (meV)	5.98 ± 0.07	9.37 ± 0.038
Γ_2 (meV)	2.06 ± 0.37	6.28 ± 0.38
χ^2	2.4057	2.1528
λ (mole-Ce/emu)	62	85

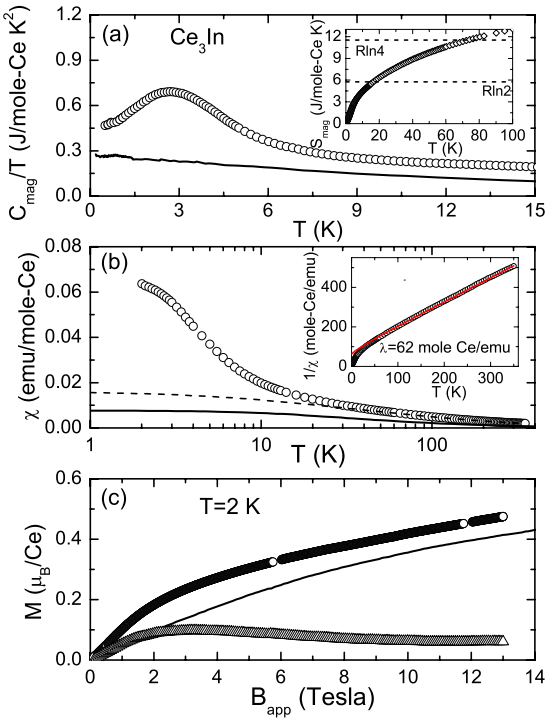

FIG. 3. (Color online) (a) The magnetic contribution to the specific heat C_{mag}/T versus T for Ce_3In. The solid line is the Kondo prediction $\gamma^K(T)$ calculated using $T_K=\Gamma_{QE}/k_B=17$ K. The inset is the magnetic entropy of Ce_3In. (b) The magnetic susceptibility $\chi(T)$ for Ce_3In. The solid line is the Kondo prediction $\chi^K(T)$ calculated using $T_K=17$ K and the low temperature Curie constant determined as described in the text. The dashed line gives the sum of the Kondo and crystal field contributions $\chi^{CEF+K}=\chi^K+(\chi^{CEF}-\chi^{LT}_{Curie})$. The inset is the inverse susceptibility together with the calculated susceptibility (solid line) $1/\chi^{HT}=1/\chi^{CEF}+\lambda$ obtained using the CEF fitting parameters in Table I. (c) The magnetization for Ce_3In. The solid line $M^K(B)$ is the Kondo calculation using $T_K=17$ K. The open triangles represent the contribution from the ferromagnetic fluctuations.

that the Kondo prediction is much smaller than the experimental value; indeed, γ_0^K is only half of $\gamma^{exp}_{0.4K}$ (Table II). The obvious explanation is that magnetic fluctuations dominate the low temperature specific heat, increasing the specific heat above the Kondo value and giving rise to the peak at 2.6 K representing the onset of short range order.

We next consider the high temperature susceptibility, comparing the measured value to the value calculated from the crystal field parameters of Table I in the inset of Fig. 3(b). A molecular-field $\lambda=62$ mole-Ce/emu has been added to compensate the reduction of the susceptibility at high temperature due to the Kondo effect $(1/\chi^{HT}=1/\chi^{CEF}+\lambda)$. At high temperatures, when the crystal field states are excited, the effective Kondo temperature T_K^{HT} is larger than the Kondo temperature of the ground state doublet. The molecular field constant is related to the effective Kondo temperature via $\lambda=T_K^{HT}/C_{5/2}$ where $C_{5/2}$ is the free ion Curie constant for cerium. This relation gives $T_K^{HT}=77$ K, which value is essentially equal to the width Γ_1 of the first excited level seen in the neutron scattering (Fig. 2 and Table I).

At low temperatures, there should be three contributions to $\chi(T)$, as well as to $M(H)$ and C_{mag}: one from the Kondo single ion impurity physics of the ground state doublet, one from the excitation of higher lying crystal field states, and one from the magnetic fluctuations. We assume the latter to be primarily ferromagnetic, for reasons discussed in Sec. IV. To carry out such an analysis, we note first that in the Cu_3Au crystal structure, the tetragonal crystal field axis (i.e., the z axis for the doublet wave functions) points perpendicular to the face containing any given face-centered cerium atom; hence there are three orthogonal tetragonal axes in the unit cell. When applying a magnetic field in a polycrystalline sample, the field will point along the tetragonal axis for $\frac{1}{3}$ of the cerium atoms but orthogonal to the tetragonal axis (in the x-y plane) for $\frac{2}{3}$ of the atoms. The effective low-temperature Curie constant is then $C_{eff}=\frac{1}{3}C^z_{eff}+\frac{2}{3}C^x_{eff}$, where $C^{z(x)}_{eff}=N(g^{z(x)}_{eff}\mu_B)^2\frac{1}{2}(\frac{1}{2}+1)/3k_B$. This is the form for a pseudo spin $\frac{1}{2}$ doublet where the CEF physics is absorbed into the effective g-factor. Here $g^{z(x)}_{eff}=\frac{12}{7}\langle J_{z(x)}\rangle$ where $\langle J_{z(x)}\rangle$ is the matrix element of the angular moment component along the $z(x)$ axis. From the CEF mixing parameter η, we determine C_{eff} to be 0.48 emu-K/mole-Ce for Ce_3In. (Table II).

To sort the low temperature susceptibility into Kondo, FM, and CEF contributions, we note that since the first CEF excited level is at 152 K, at sufficiently low temperatures the Zeeman splitting of the $\Gamma_7^{(1)}$ ground state doublet will obey a Curie law $\chi^{LT}_{Curie}=C^{LT}_{eff}/T$. Due to the Kondo effect, this Curie behavior will be replaced by the Kondo contribution χ^K, which we calculate using the same Curie constant C^{LT}_{eff} and using $T_K=17$ K [solid line, Fig. 3(b)]. The susceptibility from the combination of the ground state Kondo and the excited crystal fields will then be of the form $\chi^{CEF+K}=\chi^K+(\chi^{CEF}-\chi^{LT}_{Curie})$ where we subtract χ^{LT}_{Curie} to avoid double counting the ground state contribution. As for the specific heat, the resulting χ^{CEF+K} [dashed line in Fig. 3(b)] is much smaller than the experimental value at $T<20$ K. The excess can be viewed as the contribution from the ferromagnetic fluctuations. Taking the latter to be equal to the difference $\chi^{exp}-\chi^{CEF+K}(T)$, the FM contribution is seen to increase below 10 K in a manner characteristic of ferromagnetic short range order.

In Fig. 3(c), we exhibit the magnetization as measured up to 13 Tesla at $T=2$ K. Based on Hewson's calculation of

TABLE II. Kondo single ion model calculation for Ce_3In and Ce_3Sn.

	$\langle J_z\rangle$	$\langle J_x\rangle$	M^{sat}_{CEF}	C^{LT}_{eff}	χ^K_0 $(\frac{emu}{mole\text{-}Ce})$	γ^K_0 $(\frac{J}{mole\ Ce\ K^2})$	$\chi^{exp}_{0.4K}$ $(\frac{emu}{mole\text{-}Ce})$	$\gamma^{exp}_{0.4K}$ $(\frac{J}{mole\ Ce\ K^2})$
Ce_3In	2.0344	0.7171	0.991	0.4765	0.0076	0.256	0.064	0.467
Ce_3Sn	1.6684	0.9074	0.994	0.4086	0.0033	0.109	0.018	0.221

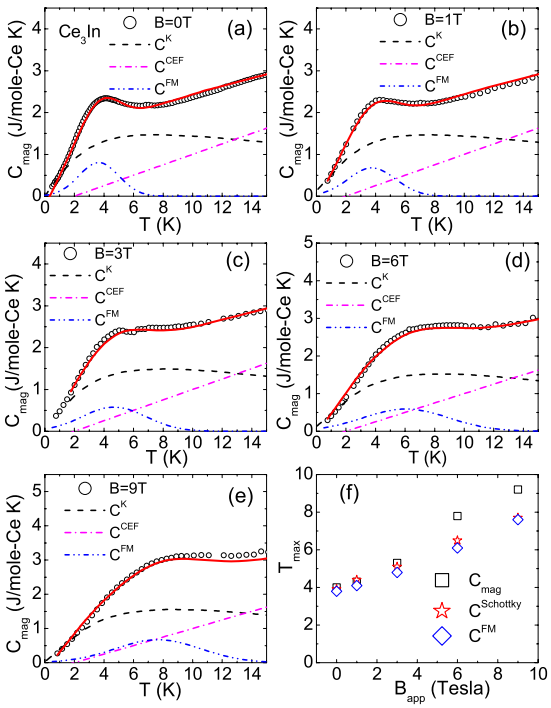

FIG. 4. (Color online) (a), (b), (c), (d), and (e): C_{mag} of Ce_3In in different applied magnetic fields. The solid line sums the three contributions (Kondo, CEF, and FM fluctuations) shown in the plot. (f): The peak position of C_{mag}, of the Gaussian contribution C^{FM} due to the FM fluctuations, and the expected peak position in the Schottky anomaly $C^{\mathrm{Schottky}}(B_{\mathrm{int}}+B_{\mathrm{app}})$ due to Zeeman splitting in the presence of an internal field B_{int}.

Kondo model,[10] we can estimate the Kondo contribution to the magnetization. Since the effective g factors differ in the z and $x-y$ directions, we calculate $M^K=\frac{1}{3}M^K(z)+\frac{2}{3}M^K(xy)$. The result is plotted as a solid line in Fig. 3(c). After subtracting the Kondo contribution, we obtain the contribution from the FM correlations (open triangles). This saturates at a relatively small field $B\sim 2.5$ Tesla with $M^{\mathrm{sat}}=0.095\ \mu_B$, which is 10 percent of the saturation value 1.0 μ_B expected based on the effective g factors.

In order to better understand these compounds, we measured the specific heat of Ce_3In under different applied fields ($B=0$, 1, 3, 6, and 9 T). The results for the magnetic contribution C_{mag} are shown in Fig. 4. The low temperature peak in C_{mag} moves to higher temperature when the field is increased. Since the peak in the Kondo contribution to C_{mag} is expected to increase with field, we plot in Figs. 4(a)–4(e) the Kondo contribution $C^K(B)$ calculated for different applied fields using the theoretical results of Sacramento and Schlottmann.[11] In calculating $C^K(B)$, we again account for the different effective g factors in the z and x-y directions. The results indicate that the Kondo contribution is not expected to alter significantly in applied fields of order 9 T, essentially because $g_{\mathrm{eff}}\mu_B B<k_B T_K$ for these fields. This makes it clear that the peak does not arise from the Kondo scattering but must be due to the FM fluctuations.

To quantify the FM contribution, we again assume that the measured magnetic specific heat is the sum of the ground-state doublet Kondo contribution $C^K(B)$, the FM contribution C^{FM}, and a contribution C^{CEF} due to the excitation of higher lying CEF states. Since the FM fluctuations appear to only contribute to the susceptibility below 10 K [Fig. 3(b)] we assume that the excess C_{mag}-$C^K(B)$ observed for $T>10$ K is primarily due to CEF excitations. Given the large linewidths of the CEF excitations seen in the neutron scattering, and concomitant large effective T_K^{HT} at high temperature, this contribution to the specific heat is much broader as a function of temperature than would be the case for a simple CEF Schottky anomaly. For simplicity, we approximate this CEF contribution as linear in temperature, with slope equal to that observed in the range 8–15 K, and we assume that since the CEF excitation energy is large, this contribution will be unaffected by fields of order 9 T. We approximate the FM contribution C^{FM} as a Gaussian, centered at a temperature that increases with field. The three contributions, Kondo, CEF, and FM, are plotted at the different fields in Figs. 4(a)–4(e). The solid lines, which represent the sum of all three contributions, fit the data very well at all fields.

We plot the Gaussian peak temperature in Fig. 4(f), where it is seen to grow linearly with field. This suggests Zeeman splitting, where at zero field the splitting arises from the internal field in the regions of FM short range order, and where the applied field increases the splitting. To determine the internal field B_{int}, we calculate the Schottky anomaly $C^{\mathrm{Schotkky}}(B_{\mathrm{int}})$ expected due to Zeeman splitting of a doublet with the same effective g-factors as we have obtained from the neutron fits; we then adjust B_{int} until the peak temperature of the Schottky anomaly is the same as that of the Gaussian peak temperature for $B=0$. This gives $B_{\mathrm{int}}=9.5$ T. We then calculate $C^{\mathrm{Schottky}}(B_{\mathrm{int}}+B_{\mathrm{app}})$ to determine peak position of the Schottky anomaly in an applied field B_{app}. As can be seen in Fig. 4(f), the Gaussian peak temperatures track the expected Zeeman splitting very closely. On the other hand, the temperature dependence of the Schottky specific heat calculated in this manner is considerably broader than the Gaussian contributions C^{FM} that are plotted in Fig. 4. This means that, while the contribution of the FM short range order to the specific heat is not of Schottky form, the increase of the Gaussian peak position is the same as the Zeeman splitting expected for a total field $B_{\mathrm{int}}+B_{\mathrm{app}}$ given the effective g factors.

The entropy of the Gaussian contribution is about 15% of Rln2 for all fields. This corresponds to the estimate obtained from the magnetization $M(B)$ where the saturation value of the FM contribution is about 10% of the value 1.0 μ_B expected for the $\Gamma_7^{(1)}$ ground state doublet for the measured value of η. Hence, the enhancement of χ_0 and γ_0 arises from magnetic fluctuations which involve 10%–15% of the $4f$ electron degrees of freedom.

B. Ce_3Sn

Using a similar analysis as for Ce_3In, the low Q data for Ce_3Sn and La_3Sn, which were collected on HET, are compared in Fig. 5 where the incident energies are $E_i=15$ meV (a) and 60 meV (b) at 4.5 K. Two excited energy levels are again observed, which correspond to crystal field excitations;

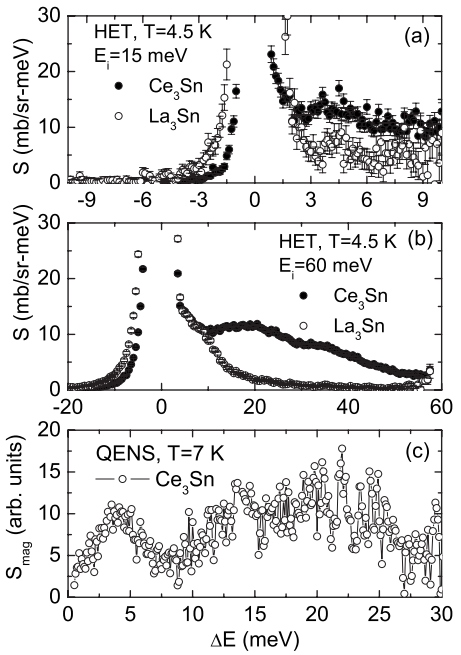

FIG. 5. Inelastic neutron scattering spectra for Ce_3Sn together with that of the nonmagnetic counterpart compound La_3Sn. The data were collected on HET and QENS. (a) E_i=15 meV and (b) E_i=60 meV. (c) Magnetic contribution of QENS spectra is obtained as described in experiment section. As for Ce_3In, the increased elastic intensity seen for La_3Sn relative Ce_3Sn for neutron energy gain arises from the larger incoherent scattering length for La compared to Ce.

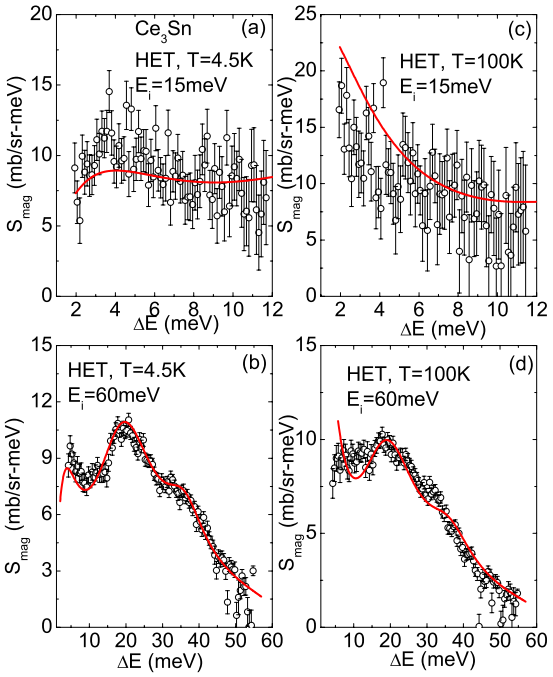

FIG. 6. (Color online) (a)-(d) Magnetic contribution S_{mag} to the inelastic neutron scattering spectra for Ce_3Sn. The temperatures and incident energies are given in the plot. The solid lines represent the CEF model.

the low energy transfer ($\Delta E < 9$ meV) spectrum exhibits obvious quasielastic scattering which arises from the Kondo effect. QENS results in Fig. 5(c) again confirms the existence of this quasielastic scattering.

In Figs. 6(a)–6(d) we display the magnetic contribution to the Ce_3Sn scattering collected from HET at 4.5 and 100 K and at two incident energies (15 and 60 meV). The CEF fits are also included (solid lines); the fits were performed simultaneously on six different spectra at different incident energies (E_i=15 meV, 35 meV, 60 meV and 100 meV), different temperatures (T=4.5, 10, 100, 150, 200, and 250 K) and different instruments (HET, LRMECS, QENS). The fitting parameters yield a similar crystal field scheme as for Ce_3In: the $\Gamma_7^{(1)}$ doublet is the ground state, $\Gamma_7^{(2)}$ is the first excited state with energy 18.5 meV, and the second excited state is the Γ_6 doublet at the energy 36.1 meV. The Kondo temperature T_K=40 K is higher than for Ce_3In, and the excited state linewidths are broader, reflecting stronger 4f-conduction hybridization.

In the same way as for Ce_3In, we determine C_{eff} to be 0.41 emu-K/mole-Ce for Ce_3In from the CEF mixing parameter η, (Table II). By using this C_{eff}, we calculate $\chi^K(T)$, $\chi^{\text{CEF}}(T)$, $\chi^{\text{CEF}+K}(T)$, $\gamma^K(T)$ and $C^K(T)$ for Ce_3Sn, comparing to the measured data in Fig. 7. The high temperature susceptibility (Fig. 7(b) inset) can again be fit with the sum of the CEF contribution calculated using the parameters of Table I and a molecular field contribution (solid line). The value λ=85 mole-Ce/emu of molecular field constant implies an effective Kondo temperature at high temperature T_K^{HT}=105 K, which again is essentially equal to the linewidth 9.4 meV of the first excited state seen in the neutron scattering (Table I).

The solid lines in Fig. 7 represent the Kondo ground state doublet contributions. In Fig. 7(b), the dashed line is $\chi^{\text{CEF}+K}(T)$. The excess due to the FM correlations has a much smaller magnitude (~0.005 emu/mol-Ce) than for Ce_3In where the FM contribution is of order 0.05 emu/mol-Ce. A similar statement holds for the FM contribution to the specific heat coefficient, which is of order 0.4 J/mol-Ce-K^2 for Ce_3In but only 0.1 J/mol-Ce-K^2 for Ce_3Sn [Figs. 3(a) and 7(a)]. Hence, the FM enhancement is smaller in Ce_3Sn than in Ce_3In, consistent with the larger value of T_K and smaller Wilson ratio.

In Fig. 7(c), we compare the magnetic specific heat C_{mag} at zero field and B=9 T for Ce_3Sn. The solid line is the Kondo contribution C^K. The specific heat does not change with field for $B < 9$ T. The most likely explanation of this is that, as discussed above, the FM correlations make a smaller contribution than in Ce_3In. The excess specific heat $C_{\text{mag}} - C^K$ seen for $T > 6$ K is presumably due to the CEF contribution, which should be even broader in temperature in Ce_3Sn than in Ce_3In due to the larger Kondo temperature.

IV. DISCUSSION

We have demonstrated that the specific heat coefficient γ observed in Ce_3In and Ce_3Sn is considerably larger than expected based on single ion Kondo physics. As mentioned in the introduction, in heavy Fermion systems where magnetic correlations are not important, the onset of coherence has

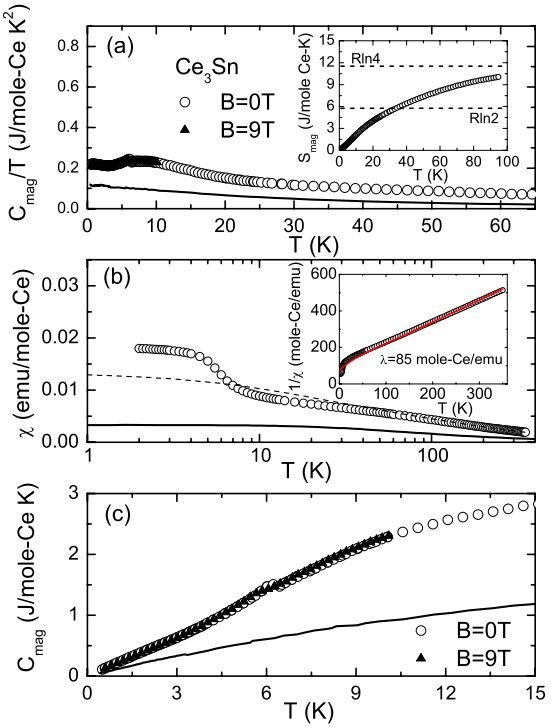

FIG. 7. (Color online) (a) the magnetic specific heat C_{mag}/T versus T at B=0 T (open circle) and B=9 T (solid triangle) for Ce_3Sn. The solid line is the Kondo contribution $\gamma^K(T)$ for T_K=40 K. The inset is the magnetic entropy. (b) Magnetic susceptibility $\chi(T)$ for Ce_3Sn. The solid line is the Kondo contribution $\chi^K(T)$ calculated with $T_K=\Gamma_{\mathrm{QE}}/k_B=40$ K and the dashed line is the sum of the Kondo and CEF contributions $\chi^{\mathrm{CEF}+K}=\chi^K+(\chi^{\mathrm{CEF}}-\chi^{\mathrm{LT}}_{\mathrm{Curie}})$. The inset is the inverse susceptibility together with the value $1/\chi^{\mathrm{HT}}=1/\chi^{\mathrm{CEF}}+\lambda$ (solid line) calculated from CEF fitting parameters in Table I. (c) C_{mag} at $B=0$ T (open circle) and $B=9$ T (solid triangle) for Ce_3Sn. The thin solid line is $C^K(T)$ calculated with T_K=40 K.

only a small effect on the specific heat.[6,7] Hence for the Ce_3X compounds, the excess specific heat must arise from magnetic correlations, reflecting the fact that the system is close to a magnetic quantum critical point.

While antiferromagnetic fluctuations may also contribute, we have based our analysis on the assumption that these correlations are primarily ferromagnetic. The evidence for this comes from the large Wilson ratios (11.5 and 7.0 for Ce_3In and Ce_3Sn, respectively), the excess magnetization seen in Fig. 3(c), which saturates in low field, and the excess susceptibility seen in Figs. 3(b) and 7(b). The existence of FM fluctuations does not necessarily imply that the magnetic ordering at the QCP will be ferromagnetic. Large FM correlations can arise in antiferromagnets if the ordered state consists of ferromagnetically aligned sheets of spins which alternate in sign in the direction perpendicular to the sheets.[15] Indeed, we have observed strong FM fluctuations above T_N in the related compound Pr_3In, which is an antiferromagnet below 12 K.[16] A possible explanation for this behavior is that AFM interactions between rare earth atoms on the face centers of the Cu_3Au structure are frustrated. If, for example, the atoms at (1/2 1/2 0) and (1/2 0 1/2) are aligned antiferromagnetically, the atom at (0 1/2 1/2) will be free to point to any direction. Ferromagnetic next-nearest-neighbor interactions could then stabilize ferromagnetism on this sublattice.[17] In any case, the FM correlations appear to be generic to this crystal structure.

In a **Q**-resolved INS experiment, the ferromagnetic correlations should show up in the vicinity of **Q**=0 riding on a background of **Q**-independent Kondo scattering. Our specific heat and magnetization results for Ce_3In suggest that these FM correlations will have 10%–15% of the total spectral weight in **Q**-space. Since the large γ and the proximity to the QCP occurs when the Kondo temperature T_K=17 K is fairly large, it is also reasonable to believe that when an appropriate control parameter (e.g., alloying parameter x in $Ce_{3-x}La_xIn$) drives this system to the QCP, the Kondo temperature T_K will remain finite, as expected for example for a spin density wave type QCP.

V. CONCLUSION

In conclusion, we have used inelastic neutron scattering to determine the crystalline electric field (CEF) splitting and Kondo energy scale in Ce_3In and Ce_3Sn. For both compounds the crystal field excitation energy is large. For Ce_3In we have separated the magnetization $M(B)$, susceptibility $\chi(T)$ and specific heat C_{mag} into contributions from the Kondo effect, from the CEF, and from FM fluctuations. The simplified model calculation for Ce_3In shows that the FM correlations make a 15% contribution to the doublet ground-state entropy and that the large γ arises mostly from the FM correlations. This suggests Ce_3In is close to a QCP. The Kondo temperature T_K is expected to remain finite at the QCP, as occurs for a spin density wave type QCP. INS experiments on single crystals of these compounds would be very interesting.

ACKNOWLEDGMENTS

We thank Vivien Zapf for her assistance in the measurement at NHMFL and Cristian Batista for his insightful comments. Research at UC Irvine was supported by the U.S. Department of Energy, Office of Basic Energy Sciences, Division of Materials Sciences and Engineering under Award No. DE-FG02-03ER46036. Work at ORNL was supported by the Scientific User Facilities Division Office of Basic Energy Sciences, U.S. DOE and was managed by UT-Battelle, LLC, for U.S. DOE under Contract No. DE-AC05-00OR22725. Work at Los Alamos National Laboratory was performed under the auspices of the U.S. DOE/Office of Science. Work at NHMFL-PFF, Los Alamos was performed under the auspices of the National Science Foundation, the State of Florida, and U.S. DOE. Work at ANL was supported by DOE-BES under Contract No. DE-AC02-06CH11357.

[1] V. T. Rajan, Phys. Rev. Lett. **51**, 308 (1983).
[2] Y. Y. Chen, J. M. Lawrence, J. D. Thompson, and J. O. Willis, Phys. Rev. B **40**, 10766 (1989).
[3] J. M. Lawrence, Y. Y. Chen, J. D. Thompson, and J. O. Willis, Physica B **163**, 56 (1990).
[4] H. Kadowaki, M. Sato, and S. Kawarazaki, Phys. Rev. Lett. **92**, 097204 (2004).
[5] H. Kadowaki, B. Fåk, T. Fukuhara, K. Maezawa, K. Nakajima, M. A. Adams, S. Raymond, and J. Flouquet, Phys. Rev. B **68**, 140402(R) (2003).
[6] J. M. Lawrence, S. M. Shapiro, J. L. Sarrao, and Z. Fisk, Phys. Rev. B **55**, 14467 (1997).
[7] J. M. Lawrence, P. S. Riseborough, C. H. Booth, J. L. Sarrao, J. D. Thompson, and R. Osborn, Phys. Rev. B **63**, 054427 (2001).
[8] I. Aviani, M. Miljak, V. Zaltić, K.-D. Schotte, C. Geibel, and F. Steglich, Phys. Rev. B **64**, 184438 (2001).
[9] G. Fischer and A. Herr, Phys. Status Solidi B **141**, 589 (1987).
[10] A. C. Hewson and J. W. Rasul, J. Phys. C **16**, 6799 (1983).
[11] P. D. Sacramento and P. Schlottmann, Phys. Rev. B **40**, 431 (1989).
[12] A. P. Murani, Phys. Rev. B **28**, 2308 (1983).
[13] E. A. Goremychkin and R. Osborn, Phys. Rev. B **47**, 14280 (1993).
[14] Experimental probes of CEF excitations can not distinguish between a positive and a negative value of B_4^4. Only the modulus is observable. Consequently the distinction between the $\Gamma_7^{(1)}$ and $\Gamma_7^{(2)}$ states is a matter of convention [A. D. Christianson, E. D. Bauer, J. M. Lawrence, P. S. Riseborough, N. O. Moreno, P. G. Pagliuso, J. L. Sarrao, J. D. Thompson, E. A. Goremychkin, F. R. Trouw, M. P. Hehlen, and R. J. McQueeney, Phys. Rev. B **70**, 134505 (2004)].
[15] J. M. Lawrence, K. Parvin, and S. M. Shapiro, J. Phys. C **19**, 2021 (1986).
[16] A. D. Christianson, J. M. Lawrence, J. L. Zarestky, H. S. Suzuki, J. D. Thompson, M. F. Hundley, J. L. Sarrao, C. H. Booth, D. Antonio, and A. L. Cornelius, Phys. Rev. B **72**, 024402 (2005).
[17] Cristian Batista (private communication).